Research Square

Preprints are preliminary reports that have not undergone peer review.
They should not be considered conclusive, used to inform clinical practice,
or referenced by the media as validated information.

A 14,400-Year Sediment and Pollen Record of Lake Erie Limnological Response to Lake Level, Lake Connectivity, and Climate

Beverly Z. Saylor

bzs@case.edu

Case Western Reserve University

Yunlang Zhang

Case Western Reserve University

Kalpani M Ratnayake

Kent State University

Onema Adojoh

Case Western Reserve University

Enriqueta Barrera

Independent Professional Geologist

John A. Peck

University of Akron

Joseph D. Ortiz

Kent State University

Article

Keywords:

Posted Date: November 9th, 2026

DOI: https://doi.org/10.21203/rs.3.rs-11245352/v1

License: This work is licensed under a Creative Commons Attribution 4.0 International License.
Read Full License

Additional Declarations: No competing interests reported.

Abstract

Lake Erie, the southernmost of the Laurentian Great Lakes, experienced major changes in climate, hydrology, and basin configuration from Late Glacial through Holocene time. We present a new ~ 14.4-thousand-year (~ 14.4 ka) sediment record for a central basin core constrained by radiocarbon and paleomagnetic secular variation ages, with pollen stratigraphy independently verifying the age model where radiocarbon ages are reversed. Five phases characterize the record: 1) low inorganic carbon (IC) from ~ 14.4–11.5 cal ka BP; 2) increasing IC after 11.5 cal ka BP, followed by pollen changes across an unconformity spanning 10.0–8.1 cal ka BP; 3) relatively high IC from 8.1 cal ka BP until 4) three stepwise decreases in IC and an increase in organic carbon (OC) between 5.3–3.5 cal ka BP; and 5) near zero IC from 3.5 cal ka BP to Present, with OC and pollen changes after ~ 2.3 cal ka BP. Comparison with a second central-basin core and lake level reconstructions indicates that climate, hydrologic connectivity, and lake level influenced sedimentary carbonate accumulation and contributed to the formation of an unconformity, a shift in the depocenter, and a mass slide.

Introduction

The Laurentian Great Lakes (LGL) and their connecting water bodies constitute the Earth's largest freshwater system [1] (Fig. 1a). They were carved by the Laurentide Ice Sheet (LIS) and received glacial meltwater until ~ 9,000 calendar yr BP (cal yr BP) [2]. During the Late Glacial and Holocene, lake levels and hydraulic connections changed in response to variations in glacial meltwater, glacioisostatic uplift, drainage pathways, and climate (e.g. [3–7]). Evidence for these changes and the limnological responses to them derive from two complementary archives: geomorphological indicators of former shorelines and sedimentary records obtained from lake cores. Comparison of these records provides an important framework for evaluating the drivers of Quaternary environmental change and the LGL's responses to it.

Lake Erie, the southernmost LGL, is particularly suited to evaluating the relationship between sedimentary records and independently reconstructed lake level histories. Lake Erie receives 87% of its water from the upper LGL (Superior, Michigan, and Huron; [8]). It is the shallowest of the LGL and the most responsive to hydrologic and environmental change (e.g. [9–14]). Evidence from past shoreline elevations and other geomorphological features, combined with methods to correct for differential glacioisostatic rebound, have established a robust history of Lake Erie's changing lake levels [15]. This history includes a period of at least 6,000 years

A.

Figure 1. Regional setting and locations of studied cores. (a)Map showing location of LGL Map created in DataWrapper (b) Map of Lake Erie showing cores analyzed in study (squares), previously studied cores (circles), and bathymetric contours (1 m).

(~ 12,300 to 6,300 cal yr BP) when Lake Erie was a closed basin and isolated from upper LGL drainage, followed by a period of high lake level in response to wetter conditions, a higher outlet sill, and the return

of upper LGL drainage [15–17]. Breach of the middle Holocene outlet sill after ~ 3,770 cal yr BP lowered lake level [15, 18] and water levels are thought to have largely stayed within historical limits since that time [14, 18–19]. These Late Glacial and Holocene lake-level changes provide independent chronological benchmarks for evaluating the timing of sedimentary change.

Among the most prominent sedimentary changes are variations in carbonate content, which ranged from ~ 25 wt% to near zero in previously studied sediment cores [15, 20–22]. These shifts were first reported over 45 years ago and since then have tentatively and variably been attributed to changes in sediment source and sedimentation rate [23], temperature and precipitation [21], influx of carbonate-undersaturated upper LGL water [15], and changes in the carbonate saturation of bottom water with the establishment of the central basin hypolimnion [20, 22]. Uncertainty regarding the timing and spatial continuity of sedimentary carbonate shifts has hindered understanding of their driving mechanisms.

Establishing a robust chronology for Lake Erie sediments has been challenging. Early studies had difficulty obtaining reliable ^{14}C age controls, due in part to the large sample sizes required by conventional radiocarbon dating and offsets caused by old, radioactively dead carbon dissolved in the lake water. Age estimates therefore relied heavily on indirect chronological approaches, including correlation of pollen assemblages and paleomagnetic secular variation (PSV) to dated records elsewhere, plus assumptions about sedimentation rate and correlation, or the timescale of PSV variations (e.g. [15, 20–21, 23–25, 32]). More recent studies using Accelerator Mass Spectrometry (AMS) radiocarbon dating have improved chronological control, while Ratnayake et al. [34] quantified freshwater reservoir corrections for the western, central, and eastern basins of Lake Erie, providing a basis for more accurate calibration of radiocarbon ages. Nevertheless, published age constraints remain sparse and cover limited portions of the sedimentary record [15, 22, 32]. Consequently, the timing and spatial continuity of major sedimentary changes in Lake Erie remain poorly constrained, limiting efforts to distinguish among climatic, hydrologic, sedimentary, and limnological controls.

Here, we develop an integrated chronology for Late Glacial and Holocene sediments from two piston cores collected along the axis of Lake Erie's central basin (Fig. 1b). Core 84a is a 10.28-m piston core collected from the deepest part of the central basin (41˚55' 53" N, 81˚ 37' 39", 25 m water depth), while LECB-1 is a previously studied 8.76-m core collected ~ 32 km east-southeast of 84a [22] (42˚ 04' 48" N, 81˚ 15' 32" W, 24 m water depth). For core 84a, we combine new AMS ^{14}C ages from shell material with chronological constraints from PSV. Pollen provides an independent constraint on the chronology, particularly near the base of the core where radiocarbon ages become progressively younger with depth. We also obtained new AMS ^{14}C ages and sediment composition data from core LECB-1 to improve its age control and facilitate correlation between the two records. Bayesian age-depth modeling integrates these chronological records and provides probabilistic age estimates for changes in sedimentary carbonate, pollen assemblages, and other sediment properties. We use the resulting chronology to evaluate the timing and stratigraphic reproducibility of major sedimentary changes between the two cores and to assess their relationship to independently dated changes in Lake Erie water levels. The integration of radiocarbon, pollen, and sedimentological evidence also provides a basis for evaluating

whether reversed radiocarbon ages near the base of core 84a reflect a dating or coring artifact or represent a true juxtaposition of older sediments on top of younger ones.

Results

Core 84a Radiocarbon Ages

No shell material suitable for radiocarbon dating was recovered from the upper 533 cm of core 84a (Fig. 2). Below this depth, we obtained 12 AMS ^{14}C ages, for which we report freshwater-reservoir-corrected calibrated age ranges at 95.4% probability (Table 1). Ages extend from 4,425–4,957 cal yr BP to 14,061–15,147 cal yr BP and generally increase or overlap with depth, from 4,840–5,282 cal yr BP at 534.5 cm to 14,061–15,147 cal yr BP at 961 cm. Below 961 cm, however, ages reverse, decreasing from 10,569–11,600 cal yr BP at 985 cm to 4,425–4,957 cal yr BP at 1,011 cm, such that the youngest age occurs at the greatest depth.

The shell ages define three chronostratigraphic groups: a Holocene group (< 8,500 cal yr BP; from 534.5–769 cm), a Late Glacial group (> 10,500 cal yr BP; from 833–961 cm), and a stratigraphically reversed group, comprising the 10,569 – 11,600 cal yr BP age at 985 cm and three ages < 6,500 cal yr BP below 1,000 cm (Table 1). The 985-cm age could potentially belong to the Late Glacial group, but this would require an unusually high sedimentation rate between 833 and 985 cm and the 14,061–15,147 cal yr BP age at 961 to be anomalously old.

Core 84a Paleomagnetic Secular Variation

Core 84a sediment contains a strong stable primary directional component after alternating field demagnetization at 15 mT (SM Table 1). The PSV inclination record varies about the geocentric axial dipole (61°) for the core site latitude through the upper 700 cm of core 84a and contains three prominent features that correlate with a regional PSV reference curve [26] (Fig. 3). Calibrated age estimates for these inclination features range from 794–1,273 cal yr BP at 129 cm to 5,604–6,177 cal yr BP at 625 cm (Fig. 2; Table 1). The PSV estimates agree with core 84a AMS ^{14}C age constraints and extend control through the upper part of the core where AMS ^{14}C ages are absent.

Below ~ 700 cm, the inclination pattern is characterized by high amplitude oscillations without counterpart in the regional reference curve or paleomagnetic records from the other LGL [27] (Fig. 3). Below 1,017 cm, negative inclination values are recorded in the three deepest samples. Similar oscillations and negative inclination values in other Lake Erie cores, including central-basin cores, were initially interpreted as evidence of a paleomagnetic reversal but later attributed to physical sediment disturbance [23, 27].

Core 84a Pollen Stratigraphy

Pollen assemblages include mixtures of coniferous and deciduous arboreal taxa (Fig. 4; SM Table 2). *Picea* (spruce), *Pinus* (pine), *Quercus* (oak), *Acer* (maple), and *Salix* (willow) each account for > 10% of total counts whereas Poaceae (grasses) is the only non-arboreal herbaceous taxon exceeding 10%. Constrained Incremental Sum of Squares (CONISS) identified four pollen zones and four subzones (Table 1).

Zone P1 is below 985 cm and thus within the interval of stratigraphically reversed ages from shells. It contains relatively high abundances of deciduous pollen, particularly *Quercus*, *Acer*, and *Salix*, and more closely resembles the Holocene P3 assemblage than the Late Glacial P2 assemblage, providing independent stratigraphic support for the inverted succession indicated by the radiocarbon ages.

Zone P2 is dominated by the conifers *Picea* and *Pinus*, with *Quercus* and Poaceae also abundant. *Picea* and *Pinus* decrease upward as *Quercus*, Poaceae, *Abies* (fir), and *Betula* (birch) increase, followed by declines of *Abies* and the deciduous taxa, and second *Picea* and *Pinus* peaks at 841 cm. The dominance of *Picea* and *Pinus* is consistent with a cold climate after the retreat of LIS and the variations in deciduous and coniferous taxa resemble pollen successions in reference cores from the southern LGL region that have been interpreted as recording fluctuations in Late Glacial climate and warming toward the Holocene [28, 29, 30, 31]. This correspondence supports interpreting the 14,061–15,147 cal yr BP shell age at 961 cm as a depositional age. In contrast, the younger Late Glacial shell age at greater depth (985 cm) is inconsistent with the pollen stratigraphy and is assigned to the reversed age group.

The P2–P3 zone boundary is tightly defined by the appearance or sharp increase of *Acer*, *Salix*, *Betula*, *Alnus*, and *Tsuga* (hemlock) between samples at 785 and 775 cm. Although the 775-cm sample was prepared using a different method (SM Table 3), the next higher sample, prepared by the original method, also shows increased deciduous pollen indicating the transition is not solely a preparation artifact (Fig. 4). The greater diversity and abundance of deciduous taxa in Zone P3 is consistent with Holocene pollen assemblages in the region and in other Lake Erie cores [32]. The abrupt transition from the conifer-dominated P2 vegetation, together with an ~ 2,000 year chronological gap between Late Glacial and Holocene age controls suggests an unconformity or very slow rate of accumulation at ~ 780 cm.

Zone P4, comprising the upper 261 cm of the core overlaps with the youngest of the PSV age controls. It is distinguished from P3 by an increase in Asteraceae (asters) and decrease in Cyperaceae (sedges) and Chenopodiaceae (goosefoot). *Alnus* (alder) and *tsuga* decrease while *salix* increases, but other arboreal taxa remain relatively stable. The changes primarily indicate differences in the type of open vegetation.

Overall, pollen zones P1, P2, and P3–P4 correspond with reversed, Late Glacial, and Holocene chronostratigraphic groups, respectively (Table 1).

Core 84a Sediment Properties

Inorganic carbon (IC), organic carbon (OC), water content, and magnetic susceptibility (MS) vary systematically with depth in core 84a (Fig. 2, SM Tables 4–7). IC values (< 0.2–3.4 wt%) agree between

Loss on Ignition (IC_{LOI}) and Elemental Analyzer (IC_{EA}) measurements and correspond to approximately 0–28 wt% $CaCO_3$ equivalent, comparable to the range of carbonate values reported previously for Lake Erie sediments [20, 21, 22, 25, 15]. Six geochemical zones are defined by sharp IC shifts that are consistent with independent radiocarbon and pollen constraints (Table 1).

Zone A (973 cm to core base) encompasses all four reversed ^{14}C ages. IC is high (~ 3 wt%) below 995 cm and decreases to ~ 1.5 wt% above 995 cm (Fig. 2). Zone B (973–855 cm) has moderately low IC values (1.5–2 wt%) and includes the oldest of the Late Glacial age control points. Zone C (855 – 585 cm) has the highest IC of the core (3–3.4 wt%) and sharp IC transitions near its upper and lower boundaries. Specifically, IC increases between 855 and 793 cm, from below the second *Picea* and *Pinus* peak in P2 to below the unconformity at the P2–P3 boundary. IC decreases sharply near the top of Zone C, marking the first of three stepwise shifts over which IC declines from 3.5 to < 0.2 wt%. The low IC at the end of each decline defines the upper boundaries of Zones C, D, and E, at 585, 513, and 390 cm, respectively. Zone F extends from 390 cm to the core top and has near zero IC (< 0.2 wt% by EA).

OC_{LOI} is consistently higher than OC_{EA}, but both methods show similar patterns. OC is relatively low in Zones A, B, and C, increases sharply through Zone D, and remains relatively high but variable through Zones E and F. OC_{EA} increases by ~ 0.6 wt% through Zone D from 0.8 to 1.4 wt%. Zone B has the lowest water content (< 25 wt%) and the highest MS (> 50) with the most pronounced values between 960–900 cm.

Core LECB-1

Five new AMS ^{14}C ages for shells from core LECB-1 supplement the six AMS ^{14}C ages previously reported by Clotts et al. [22]. Together, freshwater-reservoir-corrected, calibrated ages range from 3,990–4,506 cal yr BP to 6,796–7,236 cal yr BP with good agreement between the studies (Fig. 5; Table 1). Shell material was not recovered above 274.5 cm depth and ages increase with depth or overlap between 274.5 and 812 cm.

IC and OC patterns in core LECB-1 resemble geochemical Zones C–E in core 84a, and shell-based age controls provide chronological support for their correlation (SM Table 8). Accordingly, Zone C in LECB-1 extends from 390 cm to the core base, Zone D from 390–240 cm, and Zone E from 240–10 cm, where IC falls below 0.2 wt%. Previously published Chittick measurements resolve calcite and dolomite components, revealing structure in the carbonate decline not apparent in total IC [22] (SM Table 9). The $IC_{Ch-calcite}$ record includes a stepwise decline at 95 cm providing an alternate E–F boundary (E–F’). Most equivalent zones in core LECB-1 are approximately twice as thick as those in core 84a, whereas Zone F is absent, or substantially thinner if the E–F’ boundary is used. Zone B is also absent or not reached in LECB-1 (Fig. 6).

Core Chronology

Bayesian age-depth modeling of core 84a using rBacon [33] excluded Zone A sediment from the age-depth model because the radiocarbon, pollen, and sedimentological evidence indicates that it does not form part of the coherent depositional sequence represented by the overlying sediments. Alternative model scenarios, including those with or without the Late Glacial and PSV age controls, and with or without an unconformity at 780 cm, produced similar ages for most zone boundaries (SM Fig. 1; SM Table 10). We report the model incorporating the full set of Holocene and Late Glacial shell-based age controls from the coherent depositional sequence, PSV inclination, and an unconformity at 780 cm (Figs. 2 and 6).

The modeled age at the base of the coherent sequence (A–B boundary, 973 cm) is 13,721–15,065 cal yr BP (median 14,403 cal yr BP), while the core top (10 cm) is -75–105 cal yr BP (median – 39 cal yr BP). The modeled age for the B–C zone boundary is 10,978–12,058 cal yr (median 11,530 cal yr BP), for the slightly higher *Picea* and *Pinus* peak it is 10,655–11,700 cal yr BP (median 11,146 cal yr BP), and for the unconformity within Zone C, the modeled ages span 9,260–10,708 cal yr BP (median 9,976 cal yr BP at 780.2 cm) to 7,717–9,091 cal yr BP (median = 8,054 cal yr BP at 780 cm; Fig. 6; SM Table 10). Holocene geochemical zone-boundary ages range from 5,037–5,573 cal yr BP (median 5,338 cal yr BP) at C–D to 3,164–3,837 cal yr BP (median 3,514 cal yr BP) at E–F. The P3–P4 pollen zone boundary within Zone F has a modeled age of 1,942–2,589 cal yr BP (median 2,275 cal yr BP).

Core LECB-1 was modeled with *acc.mean* = 4 rather than the model-recommended *acc.mean* = 5 (Fig. 6, SM Table 10). This change to the a priori accumulation-rate parameter prevents a slope change at the youngest age-control point, for which there is no independent chronological evidence and which is not observed at the correlative level in core 84a. Modeled ages range from 4,630–4,855 cal yr BP (median 4,806 cal yr BP) for the C-D boundary to 3,070–3,594 cal yr BP (3,350) for the E-F boundary or 3,425–3,893 cal yr BP (median 3,674 cal yr BP) for the alternate E–F’ boundary (Fig. 3) The modeled age for the bottom of LECB-1 is 6,527–7,063 cal yr BP (median 6,804 cal yr BP).

Median ages of the C–D, D–E, and E–F boundaries are 532, 408, 164 cal yr BP younger, respectively, in LECB-1 than 84a. The 95.4% credible intervals for the C–D boundary ages do not overlap (SM Table 10). The top modeled age of LECB-1, corresponding to the E–F boundary based on total IC, is substantially older than the top modeled age of 84a, where E-F occurs at 380 cm. For *acc.mean* = 5, the C–D, D–E, and E–F boundaries are 512 to 543 cal yr BP younger in LECB-1 than 84a, but the top of LECB-1 is still ~ 3,002 cal yr BP.

Comparison to Independent Records of Lake Level

Comparison of 84a and LECB-1 chronologies with the independent Lake Erie lake level reconstruction of Lewis et al. [15] identifies five phases defined by the sediment and pollen record that associate with changes in lake level and connectivity (Figs. 6, 7). Phase boundary ages are defined by median ages in core 84a. Ages constraining lake level and their interpretation from Lewis et al. [15] are listed in SM

Table 11 after applying the reservoir correction and calibration approach used in this paper to the original ^{14}C ages.

Phase 1 — Lake Algonquin highstand (~ 14,403 to 11,530). Low IC in Zone B (~ 14,403–11,530 cal yr BP) encompasses a Lake Erie highstand, identified by a shell age of 13,460–13,099 cal yr BP and peat dated to 13,353–12,746 cal yr BP (SM Table 11, entries 8 and 9). This highstand is attributed to a period when Lake Algonquin, a glacial lake occupying the present-day Lake Michigan and Lake Huron basins, drained toward the Lake Erie basin.

Phase 2 — Basin closure and lake-level minimum (11,530 to 8,054 cal yr BP). The onset of the IC rise at 11,530 cal yr BP (B–C boundary) followed the initiation of closed-basin conditions, dated to 12,877–12,502 cal yr BP based on shells in a paleobeach deposit (SM Table 11, entry 13). The subsequent unconformity spanning ~ 9,976–8,054 cal yr BP, which represents a lake-level minimum, potentially corresponds with a lowstand inferred from acoustic evidence for a planar truncation surface in the central basin that Lewis et al. [15] interpreted as a wave-cut terrace.

Phase 3 — Closed basin and rising lake level (8,054 to 5,338 cal yr BP). High IC in Zone C persisted after the unconformity until the first of the three IC declines at ~ 5,338 cal yr BP. During this period Lake Erie was a closed basin. Lake level remained well below the outlet sill, possibly until as late as 6,607–6,215 cal yr BP and 6,937–6,495 cal yr BP, the ages for reworked shells in paleo-beach deposits (SM Table 11, entries 3 and 12). Subsequent level rise is dated to 6,660–5,590 and 6,599–5,320 cal yr BP based on organic matter overlain by beach sand (SM Table 11, entries 5 and 6).

Phase 4 — Nipissing highstands (5,338 to 3,514 cal yr BP). The three stepwise decreases in IC between ~ 5,338 and ~ 3,514 broadly overlap with two Lake Erie highstands, termed Nipissing 1 and Nipissing 2, after the Nipissing period of high-water level in the upper LGL. The C–D boundary in 84a (5,124–5,821 cal yr BP) overlaps with the post-Nipissing 1 decline (5,583–5,040 cal yr BP and 5,307–4,441 cal yr BP; Table 11, entries 10 and 11), the D–E boundary (4,556–5,097 cal yr BP) with the Nipissing 2 peak (4,872–4,533 cal yr BP, SM Table 11, entry 14), and the E-F boundary (3164–3837 cal yr BP) with the Nipissing 2 fall (4,088–3,515 cal yr BP; 3,830–3,352 cal yr BP, SM Table 1, entries 15 and 16) following the breach of the Middle Holocene (Lyle-Johnson) outlet sill.

Phase 5 — Low-IC conditions (3,514 cal yr BP to present). IC values remained near zero after the establishment of the Late Holocene (Erie-Buffalo) outlet sill lowered lake level. Changes in OC and pollen assemblages after ~ 2,302 cal yr BP indicate additional environmental changes during the late Holocene.

Discussion

The new chronology for sediments from Lake Erie's central basin was developed through the integration of appropriate freshwater reservoir correction [34] with a careful synthesis of multiple dating methods. This chronology provides a robust temporal framework for evaluating Late Glacial and Holocene

environmental change in Lake Erie and adds an important record to the regional archive of climate change.

The Late Glacial pollen record presented here is the only pollen record from offshore Lake Erie with multiple independent age constraints from ^{14}C dating. Higher-resolution pollen sampling could further refine the age estimates, but the timing of changes in deciduous and coniferous pollen is broadly consistent with the regional pollen stack for the southern LGL. Specifically, the onset of deciduous pollen expansion at 937 cm (12,845–14,223 cal yr BP), its subsequent recession at 889 cm (11,726–13,021 cal yr BP), and renewed expansion at 841 cm (10,655–11,700 cal yr BP) are consistent with the timing of regional Bølling–Allerød warming (14.0 ± 1.2 cal ka BP), Younger Dryas cooling (12.6 ± 0.4 cal ka BP), and renewed Holocene warming (11.6 ± 0.5 cal ka BP), respectively, identified from a stack of five dated pollen records from the southern LGL region [31].

The inferred unconformity at 780 cm, spanning 9,976– 8,054 cal yr BP, is shorter in duration than other intervals interpreted as periods of low sediment accumulation in central and eastern basin Lake Erie cores, which are dated by pollen to have begun before 12,000 cal yr BP and extended to ~ 8,000 cal yr BP [15]. The timing indicates that the minimum lake level during the Late Glacial to early Holocene lowstand occurred thousands of years after drainage from the upper LGL was routed around Lake Erie, suggesting that reduced LGL inflow was not the primary cause. Instead, the timing is consistent with enhanced aridity and evaporation after the establishment of closed-basin conditions. A broadly synchronous period of lake-level fall and vegetation reorganization in the eastern United States in the Lake Huron basin that established closed-basin conditions in two intervals between 9,500–9,300 and 9,000–8,400 cal yr BP provides independent regional evidence for substantially reduced early Holocene effective moisture [35, 36, 37].

The high abundance of *Quercus*, and expansion of *Tsuga*, *Betula*, *Alnus*, and *Salix* across the P3.1–P3.2 overlaps with Nipissing 2 consistent with the establishment of forested wetlands during the highstand [38]. The pollen transition at the P3–P4 boundary reflects a more open landscape with marsh vegetation around Lake Erie being replaced by shrub communities, possibly indicating a reduction in moisture availability that is controlled by both climate and lake level [19, 38–39].

The chronology provides a framework for testing hypotheses about the controls on sediment composition and provides evidence for spatial variation in sediment accumulation. Periods of low sedimentary carbonate, as indicated by low IC, overlap with periods of high lake level and open-basin conditions (Figs. 6 and 7). This pattern is consistent with the suggestion by Lewis et al. [15] that low sedimentary carbonate resulted from the inflow of cooler, carbonate-undersaturated water from the upper LGL, combined with lower evaporation as water moved more rapidly through the open basin. However, the timing of IC changes suggests that variations in source water chemistry and evaporation do not fully account for when IC decreases occurred. The Late Glacial period of low IC may have began before the Algonquin influx and ended after it [15]. Similarly, the final mid-Holocene stepwise decline of IC to near zero values (E–F boundary) coincided with lake-level fall *after* the Nipissing transfer of upper

LGL drainage back to Lake Erie, which began as early as 6,300 cal yr BP and was complete by 4,190 cal yr BP [15] (Fig. 7).

Delorme [20] documented a central-basin IC-depletion horizon from ~ 1.5–0 wt%, equivalent to the E–F boundary, and showed that no ostracod carapaces were present above the boundary, in sediments likely equivalent to Zone F, whereas only ostracod taxa capable of surviving periods of low oxygen were present below the boundary, in sediments likely equivalent to Zone E. Delorme [20] attributed the loss of carbonate, including carbonate shells, to bottom-water and pore-water acidification and calcite dissolution, as occurs in the central-basin hypolimnion today [40]. This explanation is consistent with the timing of the IC decline because falling lake levels would reduce hypolimnion thickness without substantially reducing the area of surface water available for photosynthesis, thereby reducing the buffer against seasonal oxygen depletion and acidification resulting from the decomposition of organic matter [9]. Thus, carbonate dissolution may have been exacerbated by lake-level fall associated with the establishment of the modern outlet sill, and it may also have contributed to earlier IC declines. The timing of the rise in OC and substantial decrease in IC leading to the C–D boundary is consistent with the hypothesis of Clotts et al. [22] that the establishment of a central basin hypolimnion with low pH bottom waters during Nipissing 2 contributed to IC decline. The timing is also consistent with increasing hypoxia and acidification during the early stages of post-peak lake-level fall (Fig. 7), which, together with a change in influx from the upper LGL might explain the more limited or absent IC and OC change during the Nipissing 1. Because the deeper eastern basin does not experience seasonal declines in dissolved oxygen, sediments from this setting may provide a record of changes in water influx that is less sensitive to carbon cycle dynamics of the hypolimnion. Comparing the deeper-basin record with the central-basin IC and ostracod records could therefore help distinguish changes in hydrologic inputs from carbonate dissolution associated with hypoxia and acidification.

Delorme [20] attributed an eastward decrease in the depth to the IC-depletion horizon to an eastward expansion of hypoxia across the central basin, assuming it to have occurred over thousands of years. Cores 84a and LECB-1 also document an eastward decrease in the thickness of IC-depleted late Holocene sediment from 380 to 10 cm, but the age ranges for the depletion event overlap, or differ by ~ 501 cal yr with *acc.mean* = 5 (SM Table 10). Assuming that the difference in Zone F thickness is not a coring artifact, the eastward decrease in thickness may reflect a change in the location of the depocenter. Delorme's observations are for benthos cores, which are less likely to have disturbed the sediment, providing some support for interpreting the thickness difference as a depositional feature rather than a coring artifact. Under this interpretation, the depocenter may initially have been located closer to LECB-1, with higher accumulation rates there than at the 84a location. Following lake-level fall associated with establishment of the modern outlet sill, the LECB-1 site may have become an area of much reduced sediment accumulation while the locus of sediment accumulation moved closer to the 84a site.

The integration of PSV, pollen, and sedimentological data, when considered in light of previously studied, long central basin cores with similar patterns of change, suggests that the stratigraphically reversed Late

Glacial and Middle Holocene shell ages in Zone A, near the base of core 84a, need not be rejected as unreliable or attributed to a coring artifact. One previously studied core, 13156, has IC patterns very similar to 84a, including relatively high IC near its base that resembles Zone A [21] (Fig. 1b). Although core 13156 lacks age constraints, Mudroch et al. [21] noted relatively warm-water mollusk taxa from this interval consistent with the Middle Holocene carbonate-enriched, closed-basin sediment identified in Zone A. Creer et al. [23] documented oscillatory and negative PSV inclination patterns from two cores, 13193 and 13194, that they interpreted as evidence for a possible paleomagnetic reversal. Morris and Carmichael [27] subsequently documented negative inclination values in core EK, located approximately midway between cores 13194 and 84a, but interpreted high differences in measurements from the same horizons as evidence for post-depositional mechanical deformation. They noted several characteristics of the deformation as consistent with gravitationally induced creep and slumping, including evidence for relatively uniform southerly overturning consistent with movement from north to south, but favored a glaciogenic origin, because the deformed interval was positioned near the inferred glacial-postglacial boundary. Our results show similar inclination variations that also are positioned below the Late Glacial-Holocene unconformity, but they support an alternative interpretation because the disrupted inclination directions occur above and across a juxtaposition of relatively coherent Late Glacial and Holocene deposits over a reversed sequence of younger Late Glacial and underlying Middle Holocene sediment. Because the underlying Middle Holocene sediment substantially postdates glacial influence in Lake Erie, the deformation cannot be attributed to glacial loading or deformation. Instead, the stratigraphic relationships are consistent with emplacement of relatively coherent Late Glacial and Holocene sediment over deformed younger sediment during a mass slide. The broad coincidence of this event with the Nipissing 2 period of elevated lake level supports a possible relationship between mass movement and Middle Holocene lake-level rise.

Materials and Methods

Core collection

Core 84a was collected by BZS and Dr. Enriqueta Barrera during a 2002 lake survey by the Canadian Coast Guard Research Vessel HMS Limnos (Fig. 1b). The core was cut into 1.5 m sections on the ship and transported to Ohio where whole core magnetic susceptibility was measured at 3 cm intervals using a Bartington Instruments MS2 meter and a MS2C 72 mm loop sensor at the University of Akron. The core sections were then split lengthwise after which magnetic susceptibility was measured every centimeter with a Bartington MS2E high resolution surface scanning sensor (SM Table 6). One half of the split core was subsampled at 2 cm intervals for wet and dry mass measurements (SM Table 7). The other half was subsampled at 8 cm intervals into 5.28 cm^3 plastic boxes for paleomagnetic measurements. Portions of dried samples were wet-sieved at approximately 50-cm intervals and examined for mollusk and ostracod shells.

Radiocarbon Dating

Shell carbonate was selected for radiocarbon dating from previously picked samples and by additional sieving and picking of bagged samples and archived, intact core. Shell samples, including mollusks (typically *Valvata* gastropods or *Sphaerium* and *Pisidium* clams), mixed ostracods, and in some cases mixtures of clams and ostracods, were picked from 84a and LECB-1 and sent to the National Ocean Sciences Accelerator Mass Spectrometry facility (NOSAMS) for ^{14}C analysis. Raw ^{14}C ages were reservoir-corrected and calibrated in OxCal 4.4 [41] using the central-basin freshwater reservoir correction of 676 ± 52 ^{14}C yr reported by Ratnayake et al. [34] and the IntCal 20 calibration curve [42]. Calendar ages are reported as ranges at 95.4% probability (Table 1).

Paleomagnetic Secular Variation Dating

The paleomagnetic cube subsamples were measured for both low and high frequency magnetic susceptibility using a Bartington Instruments MS2B sensor. The natural remanent magnetization (NRM) of the samples was then measured on a Molspin magnetometer set to long spin and using 6 measurement directions to calculate the declination, inclination and intensity of each sample. Next, 13 representative pilot samples were selected from the length of the core and step-wise AF demagnetized and remeasured on the Molspin after each demagnetization step. Based on the demagnetization plots, a 15 mT demagnetization field was determined best suited to yield the primary magnetic directional component, thus all samples were demagnetized at 15 mT and the NRM remeasured. Because the 84a core sections were not aligned with each other during coring it was only possible to obtain a downcore inclination profile and not a declination profile (SM Table 1, Fig. 3). The resulting 84a inclination profile was then correlated to the regional composite inclination curve for the eastern US [26]. Next the old-carbon corrected radiocarbon ages from the regional curve were transferred to core 84a along three correlative tie-lines. The regional composite curve is based upon three lakes in western PA and NY located only 150–250 km from the 84a core site. Because of the close proximity of these records any age difference due to westward drift of non-dipole features between the sites is considered negligible. To account for the average age difference of PSV features in the three records that comprise the regional curve [26], we apply an error of +/- 100 years to the PSV ages correlated to core 84a. The transferred radiocarbon ages were calibrated in OxCal 4.4 [41] without an additional freshwater reservoir correction.

Pollen Analysis

Twenty samples of ~ 3 g each were sent to Global Geolab in Alberta, Canada for pollen separation using HCl (40%) and HF (10%) to remove carbonate and siliciclastic minerals and Sodium Polytungstate (SPT) for density separation. Pollen counts were conducted by standard techniques based on traverses under an Olympus BX35F microscope with 20x magnification (SM Table 2, Fig. 4). A minimum of 300 grains was counted for slides with very good recovery and 100 grains for slides with Fair and Poor recovery. Three additional ~ 3 g samples from an interval with poor recovery were processed with higher HCl, centrifuged three times, and filtered with 10 µm mesh to increase separation of pollen and non-pollen palynomorphs (SM Table 3). The pollen percentages presented here retain the original taxonomic determinations. Because some northern temperate taxa may have overlapping pollen morphological

characteristics, low-abundance taxa with rare occurrences should be interpreted cautiously and are not used by themselves as indicators of vegetation change.

Sediment Properties

IC and OC were measured by elemental analysis (EA) at ~ 50 cm intervals for core 84a and by LOI at 2 cm intervals for cores 84a and LECB-1 (SM Tables 4, 5, and 8). Samples weighing ~ 0.5 g were collected from the archived core sections and sent to the University of Minnesota for EA analysis. Loss-on-ignition (LOI) was measured at Kent State University using stored dried samples from both cores. The LOI was measured after 48 hours at 550°C and 2 hours at 850°C and OC_{LOI} was calculated according to OC_{LOI} = $0.39xLOI_{550}$-0.28. IC_{LOI} was calculated as $IC_{LOI} = (LOI_{850}\text{-}LOI_{550})*M_C/M_{CaCO3}$, where M is molecular weight.

OC_{LOI} is high relative to OC_{EA} and relative to OC for LECB-1 reported by Clotts et al. [22]. OC_{LOI} likely includes some combusted water as there was no initial low temperature heating step [43]. In addition, OC_{LOI} and corresponding IC_{LOI} measurements from < 330 cm in 84a exhibit an abrupt, mirrored increase in LOI_{550} and decrease in LOI_{850} that is not seen in total LOI nor in OC_{EA}. Adjustment of + 0.5% and − 0.5% were applied to IC_{LOI} and OC_{LOI}, respectively to bring them into alignment with pre-shift values and the EA values for IC. This adjustment is for visualization, the EA values were used to define boundaries of stratigraphic change.

Previously published Chittick measurements [22] resolve the partitioning of calcite and dolomite in total carbonate. IC in calcite peaks at ~ 2.25 wt% and decreases in three stepwise shifts whereas IC in dolomite remains steady at about 0.75 wt% until the upper 30 cm above which $IC_{Ch-dolomite}$ and $IC_{Ch-total}$ decrease to < 0.2 wt%. For consistency with core 84a where only measurements of total IC are available, we use $IC_{Ch-total}$ and IC_{LOI} to define boundaries of stratigraphic change. These are similar to $IC_{Ch-total}$ until it declines to < 0.2 wt%, which we identify as an alternate Zone E–F boundary.

Age-Depth Modeling

To evaluate the age-depth relationship and estimate the ages of geochemical and pollen zone boundaries, Bayesian age-depth modeling was conducted using rBacon v. 3.1.0 [33] with the IntCal20 calibration curve [42]. Modeling of core 84a was conducted the Holocene age control points alone, with and without PSV, and for the stratigraphically coherent Late Glacial and Holocene age control points, excluding the four reversed ^{14}C ages from depths below 973 cm.

The model-recommended a priori mean accumulation-rate parameter, represented by the variable *acc.mean*, differed for the models with only Holocene age controls (acc.mean = 10 year/cm) and those with the Holocene and Late Glacial age controls (acc.mean = 20 year/cm, the default). In rBacon, *acc.mean* is expressed as the inverse of the conventional sediment accumulation rate, such that higher values represent slower sediment accumulation. The higher recommended a priori value (i.e., slower inferred accumulation) for the Late Glacial through Holocene sequence is influenced in part by the large

age gap, ~ 2,000 cal yr, between the highest Late Glacial age control and the lowest Holocene age control, which represents an interval with relatively slow sediment accumulation. We therefore modeled the age–depth relationship with and without an unconformity.

For LECB-1, *acc.mean* = 4 year/cm was used rather than the model-suggested prior of *acc.mean* = 5 year/cm to provide a moderate degree of smoothing in the age-depth model while accommodating all the calibrated age constraints, particularly those at greater depth. Thus, the prior helps prevent a change in accumulation rate above the youngest age-control point without forcing the older portion of the core away from the oldest control point (Fig. 6, SM Table 2).

Comparison to Lake Level History

Age ranges for geochemical and pollen zone boundaries based on the Bayesian age models were compared with the lake-level history of Lewis et al. [15]. This model is based on a compilation of paleo-shoreline indicators and modeled outlet sill elevations and identifies periods of open- and closed-basin conditions. The compiled 14C dates in the lake-level history of Lewis et al. [15] were recalibrated in OxCal 4.4 [41] using IntCal 20 calibration curve [42] after correcting shell-based ^{14}C ages for the central basin Lake Erie Fresh Water Correction Factor (FWRC) from Ratnayake et al. [34] (SM).

Data Availability

All data generated or analyzed during this study are included in this published article and its Supplementary Information files.

Declarations

Competing Interests

There are no competing interests to report.

Funding

Declaration

This work was supported by an Ohio Sea Grant awarded to B.Z.S., an EPA grant on which B.Z.S. served as a collaborator, and departmental funds from Case Western Reserve University awarded to B.Z.S. and from Kent State University awarded to J.D.O.

Author Contribution

B.Z.S. conceived and designed the study, conducted the investigation, analyzed the data, and wrote the original manuscript. Y.Z. conducted the pollen data collection, data analysis, and interpretation, and

contributed to manuscript writing. K.M.R. contributed to the OC, IC and radiocarbon dating data collection, analysis, and interpretation, and contributed to manuscript writing. O.A. designed the pollen data collection and contributed to pollen data analysis and interpretation. J.A.P. designed the PSV data collection, analyzed and interpreted the PSV data, and contributed to manuscript writing. J.D.O. contributed to the study design, data generation, and data analysis, and reviewed and edited the manuscript. All authors contributed to interpretation of the results, reviewed and revised the manuscript critically for important intellectual content, and approved the final version.

Acknowledgement

We thank Zachary Jencks for contributions to core analysis, particularly magnetic analyses, as a Master of Science student at Case Western Reserve University.

Data Availability

All data generated or analyzed during this study are included in this published article and its Supplementary Information files.

Table 1

Tables 1 is available in the Supplementary Files section.

References

1. Sterner, R. W. The Laurentian Great Lakes: a biogeochemical test bed. *Annu. Rev. Earth Planet. Sci.* **49**, 201–229. 10.1146/annurev-earth-071420-051746 (2021).
2. Breckenridge, A. The Lake Superior varve stratigraphy and implications for eastern Lake Agassiz outflow from 10,700 to 8900 cal ybp (9.5–8.0 14C ka). *Palaeogeogr Palaeoclimatol Palaeoecol*. **246**, 45–61. 10.1016/j.palaeo.2006.10.026 (2007).
3. Calkin, P. E. & Feenstra, B. H. Evolution of the Erie-basin Great Lakes. In Quaternary Evolution of the Great Lakes (eds Karrow, P. F. & Calkin, P. E.) 149–170Geological Association of Canada, Special Paper 30, (1985).
4. Croley, I. I., Lewis, C. M. & T. E. & Warmer and drier climates that make terminal Great Lakes. *J. Great Lakes Res.* **32**, 852–869 (2006). 10.3394/0380–1330(2006)32[852:WADCTM]2.0.CO;2.
5. Wilcox, D. A., Thompson, T. A., Booth, R. K. & Nicholas, J. R. Lake-level variability and water availability in the Great Lakes. *U S Geol. Surv. Circular*. **1311** 10.3133/cir1311 (2007).
6. Lewis, C. F. M. & King, J. W. Introduction to Holocene water levels and paleo-hydrology of the Laurentian Great Lakes. *J. Paleolimnol*. **47**, 293–297 (2012).

7. Herdendorf, C. E. Research overview: Holocene development of Lake Erie. *Ohio J. Sci.* **112**, 24–36 (2013).
8. Quinn, F. H. & Guerra, B. Current perspectives on the Lake Erie water balance. *J. Great Lakes Res.* **12**, 109–116. 10.1016/S0380-1330(86)71705-X (1986).
9. Charlton, M. N. Hypolimnion oxygen consumption in lakes: discussion of productivity and morphometry effects. *Can. J. Fish. Aquat. Sci.* **37**, 1531–1539. 10.1139/f80-198 (1980).
10. Dusini, D. S., Foster, D. L., Shore, J. A. & Merry, C. The effect of Lake Erie water level variations on sediment resuspension. *J. Great Lakes Res.* **35**, 1–12. 10.1016/j.jglr.2008.04.001 (2009).
11. Scavia, D. et al. Assessing and addressing the re-eutrophication of Lake Erie: central basin hypoxia. *J. Great Lakes Res.* **40**, 226–246. 10.1016/j.jglr.2014.02.004 (2014).
12. Watson, S. B. et al. The re-eutrophication of Lake Erie: harmful algal blooms and hypoxia. *Harmful Algae*. **56**, 44–66. 10.1016/j.hal.2016.04.010 (2016).
13. Tellier, J. M. et al. Widespread prevalence of hypoxia and the classification of hypoxic conditions in the Laurentian Great Lakes. *J. Great Lakes Res.* **48**, 13–23 (2022).
14. Wiles, G. C., Devereux, K., Gaglioti, B. V. & D'Arrigo, R. D. A 420-year perspective on winter Lake Erie levels. *Geophys. Res. Lett.* 50, e; (2022). GL099911 10.1029/2022GL099911 (2023).
15. Lewis, C. F. M., Cameron, G. D. M., Anderson, T. W., Heil, C. W. & Gareau, P. L. Lake levels in the Erie Basin of the Laurentian Great Lakes. *J. Paleolimnol*. **47**, 493–511. 10.1007/s10933-012-9578-5 (2012).
16. Tinkler, K. J., Pengelly, J. W., Parkins, W. G. & Terasmae, J. Evidence for high water levels in the Erie basin during the Younger Dryas Chronozone. *J. Paleolimnol*. **7**, 215–234. 10.1007/BF00181715 (1992).
17. Holcombe, T. L. et al. Revised Lake Erie postglacial lake level history based on new detailed bathymetry. *J. Great Lakes Res.* **29**, 681–704. 10.1016/S0380-1330(03)70470-5 (2003).
18. Pengelly, J. W., Tinkler, K. J., Parkins, W. G. & McCarthy, F. M. 12 600 years of lake level changes, changing sills, ephemeral lakes and Niagara Gorge erosion in the Niagara Peninsula and Eastern Lake Erie basin. *J. Paleolimnol*. **17**, 377–402. 10.1023/A:1007946401036 (1997).
19. Finkelstein, S. A. & Davis, A. M. Paleoenvironmental records of water level and climatic changes from the middle to late Holocene at a Lake Erie coastal wetland, Ontario, Canada. *Quat Res.* **65**, 33–43. 10.1016/j.yqres.2005.08.021 (2006).
20. Delorme, L. D. & Lake Erie oxygen; the prehistoric record. *Can. J. Fish. Aquat. Sci.* **39**, 1021–1029. 10.1139/f82-137 (1982).
21. Mudroch, A., Zeman, A. J. & Kalas, L. L. Calcium carbonate in postglacial Lake Erie sediment. *J. Great Lakes Res.* **8**, 711–718. 10.1016/S0380-1330(82)72011-8 (1982).
22. Clotts, R. A. et al. Middle Holocene hydrologic change and hypolimnion formation in Lake Erie. *J. Great Lakes Res.* **31**, 296–308. 10.1016/S0380-1330(05)70322-1 (2005).

23. Creer, K. M., Anderson, T. W. & Lewis, C. F. M. Late Quaternary geomagnetic stratigraphy recorded in Lake Erie sediments. *Earth Planet. Sci. Lett.* **31**, 37–47 (1976).
24. Fritz, P., Anderson, T. W. & Lewis, C. F. M. Late-Quaternary climatic trends and history of Lake Erie from stable isotope studies. *Science* **190**, 267–269. 10.1126/science.190.4211.267 (1975).
25. Lewis, C. F. & Anderson, T. W. Stable isotope (O and C) and pollen trends in eastern Lake Erie, evidence for a locally-induced climatic reversal of Younger Dryas age in the Great Lakes basin. *Clim. Dyn.* **6**, 241–250. 10.1007/BF00193537 (1992).
26. King, J. W. & Peck, J. A. Kluwer Academic Publishers, Use of paleomagnetism in studies of lake sediments. In Tracking Environmental Change Using Lake Sediments: Volume 1: Basin Analysis, Coring, and Chronological Techniques (eds Last, W. M. & Smol, J. P.) 371–389; (2001). 10.1007/0-306-47669-X_14
27. Morris, W. A. & Carmichael, C. M. The Erieau excursion revisited. *Can. J. Earth Sci.* **30**, 1741–1748 (1993).
28. Prentice, I. C., Bartlein, P. J. & Webb, I. I. I. Vegetation and climate change in eastern North America since the last glacial maximum. *Ecology* **72**, 2038–2056 (1991).
29. Yu, Z. Ecosystem response to Lateglacial and early Holocene climate oscillations in the Great Lakes region of North America. *Quat Sci. Rev.* **19**, 1723–1747 (2000).
30. Gill, J. L., Williams, J. W., Jackson, S. T., Donnelly, J. P. & Schellinger, G. C. Climatic and megaherbivory controls on late-glacial vegetation dynamics: a new, high-resolution, multi-proxy record from Silver Lake, Ohio. *Quat Sci. Rev.* **34**, 66–80. 10.1016/j.quascirev.2011.12.008 (2012).
31. Watson, B. I. et al. Temperature variations in the southern Great Lakes during the last deglaciation: comparison between pollen and GDGT proxies. *Quat Sci. Rev.* **182**, 78–92 (2018).
32. Lewis, C. F. M., Cameron, G. D. M., Barnett, P. J. & Todd, B. J. Onshore–offshore correlation of central Lake Erie glacial deposits. *Can. J. Earth Sci.* **60**, 1404–1427. 10.1139/cjes-2023-0017 (2023).
33. Blaauw, M. & Christen, J. A. Flexible paleoclimate age-depth models using an autoregressive gamma process. *Bayesian Anal.* **6**, 457–474. 10.1214/11-BA618 (2011).
34. Ratnayake, K. M., Clotts, R., Barrera, E. C., Saylor, B. Z. & Ortiz, J. D. A pre-bomb radiocarbon freshwater reservoir correction for the Laurentian Great Lakes. *J. Paleolimnol*. **70**, 175–192. 10.1007/s10933-023-00289-6 (2023).
35. Shuman, B., Bartlein, P., Logar, N., Newby, P. & Webb, T. III Parallel climate and vegetation responses to the early Holocene collapse of the Laurentide Ice Sheet. *Quat Sci. Rev.* **21**, 1793–1805 (2002).
36. Lewis, C. F. M. et al. Dry climate disconnected the Laurentian Great Lakes. *Eos Trans. AGU*. **89**, 541–542. 10.1029/2008EO520001 (2008).
37. Brooks, G. R., Medioli, B. E. & Telka, A. M. Evidence of early Holocene closed-basin conditions in the Huron-Georgian basins from within the North Bay outlet of the upper Great Lakes. *J. Paleolimnol*. **47**, 469–492. 10.1007/s10933-010-9408-6 (2012).

38. Cordero Oviedo, C., Loder, A. L., Byun, E. & Finkelstein, S. A. Past vegetation and hydrological change since the Middle Holocene in a Lake Erie riparian marsh provide a guide for ecosystem restoration. *Quat Res.* **130**, 45–58. 10.1017/qua.2025.10038 (2026).
39. Booth, R. K., Notaro, M., Jackson, S. T. & Kutzbach, J. E. Widespread drought episodes in the western Great Lakes region during the past 2000 years: geographic extent and potential mechanisms. *Earth Planet. Sci. Lett.* **242**, 415–427. 10.1016/j.epsl.2005.12.028 (2006).
40. Matisoff, G., Lindsay, A. H., Matis, S. & Soster, F. M. Trace metal mineral equilibria in Lake Erie sediments. *J. Great Lakes Res.* **6**, 353–366. 10.1016/S0380-1330(80)72117-2 (1980).
41. Ramsey, C. B. Bayesian analysis of radiocarbon dates. *Radiocarbon* **51**, 337–360. 10.1017/S0033822200033865 (2009).
42. Reimer, P. J. et al. The IntCal20 Northern Hemisphere radiocarbon age calibration curve (0–55 cal kBP). *Radiocarbon* **62**, 725–757. 10.1017/RDC.2020.41 (2020).
43. Santisteban, J. I. et al. Loss on ignition: a qualitative or quantitative method for organic matter and carbonate mineral content in sediments? *J. Paleolimnol*. **32**, 287–299. 10.1023/B:JOPL.0000042999.30131.5b (2004).

Figures

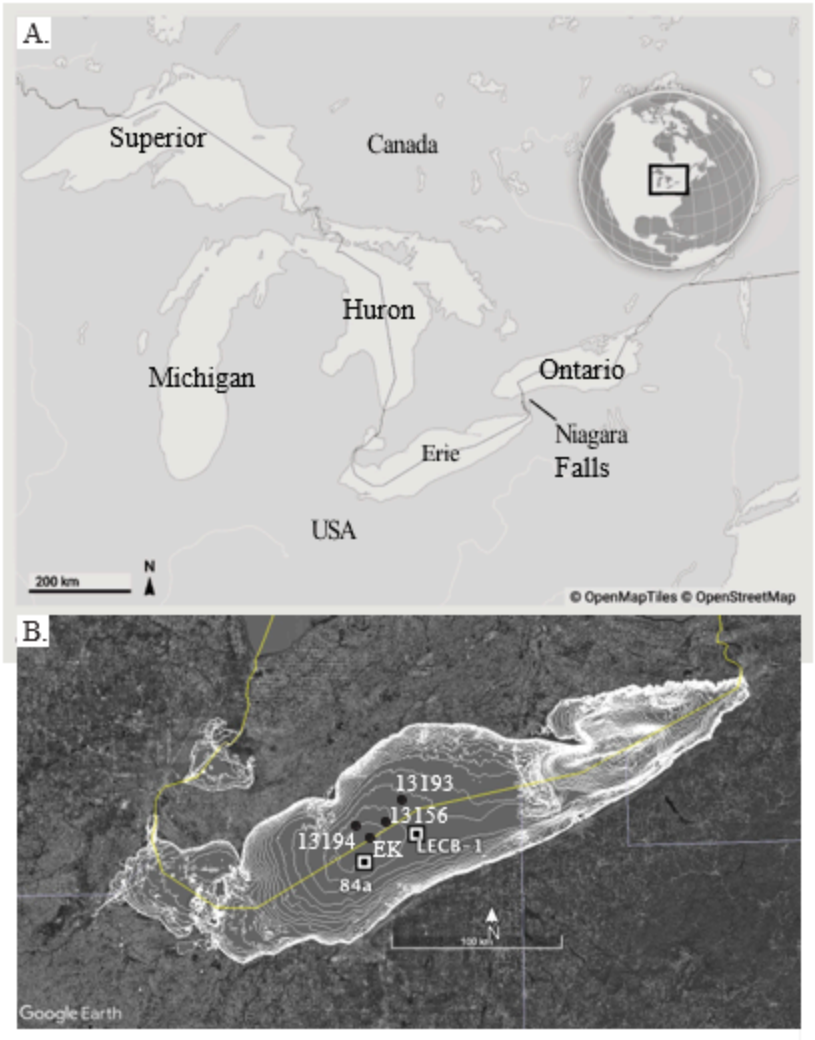


Figure 1

Regional setting and locations of studied cores. (a)Map showing location of LGL Map created in DataWrapper (b) Map of Lake Erie showing cores analyzed in study (squares), previously studied cores (circles), and bathymetric contours (1 m).

Image not available with this version

Figure 2

This image is not available with this version.

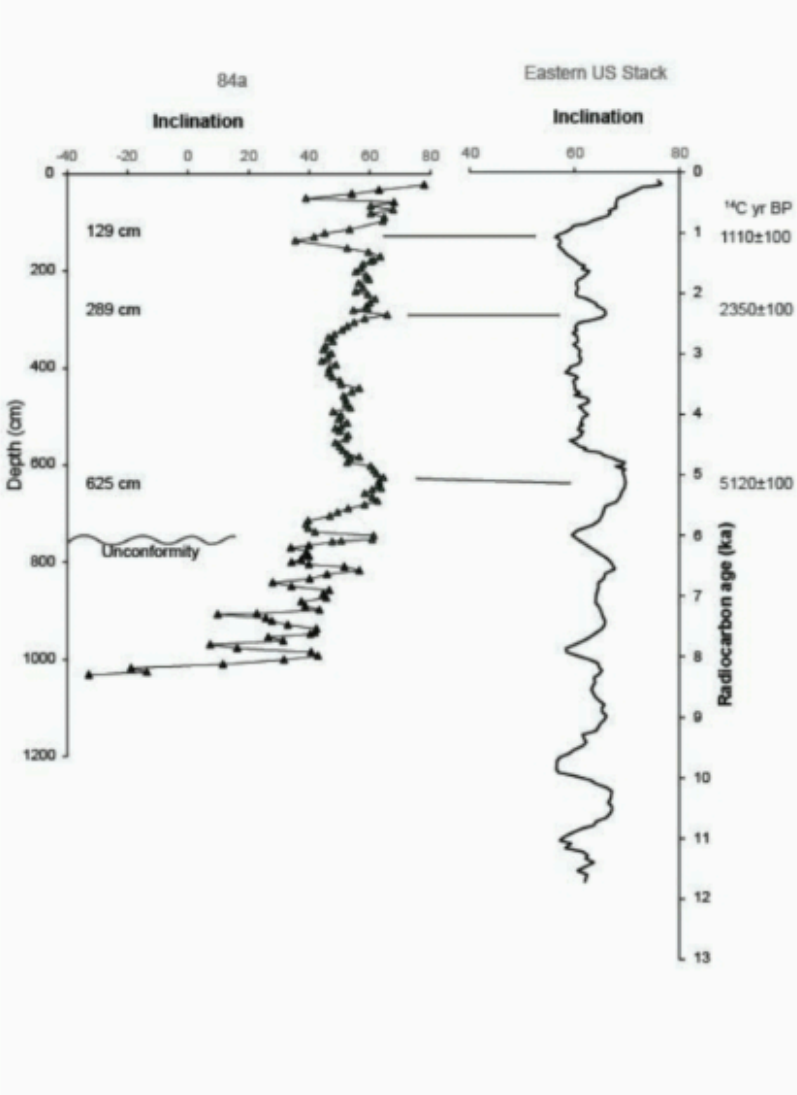


Figure 3. Comparison of core 84a PSV inclination at 15 mT with the Eastern U.S. stack. Lines indicate correlations between PSV features used to estimate ages in core 84a. Eastern U.S. stack data are from King and Peck (2001).

Figure 3

See image above for figure legend.

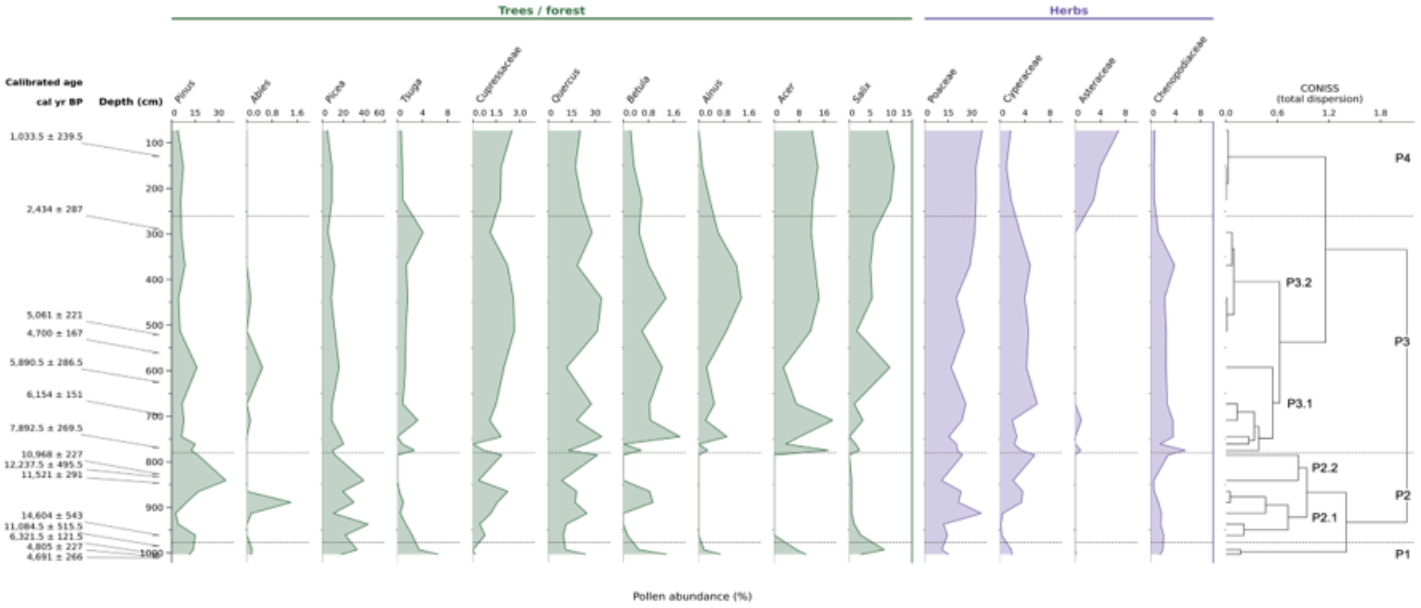


Figure 4

Pollen diagram for core 84a. Percentages are relative to total counts. Calibrated ages for control points are mean values. See Table 1 for 95.4% range.

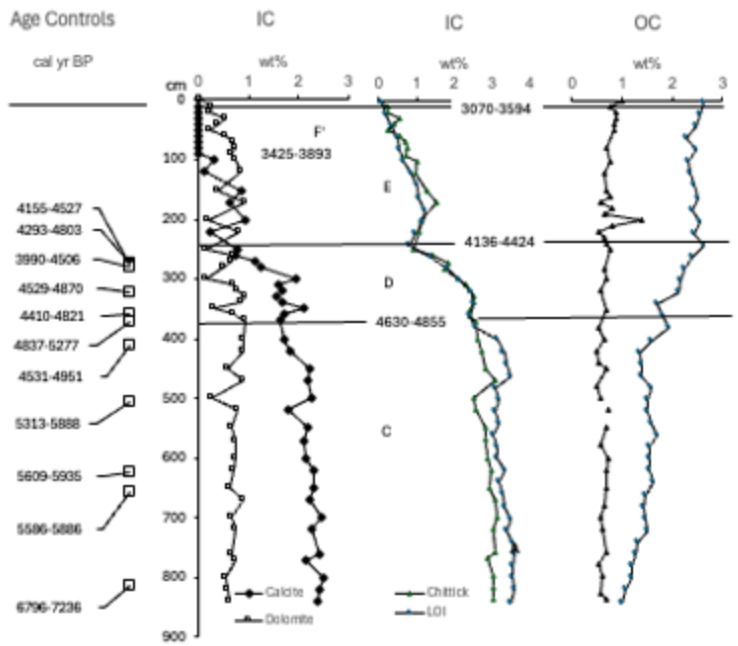


Figure 5

Sediment-property and age-control data for core LECB-1. Bayesian-modeled ages

from rBacon for geochemical-zone boundaries (C–F, solid lines) are shown, as are ages for

control points calibrated in OxCal (squares). IC and OC LOI values are from this study. All other compositional data and some age control points are from Clotts et al. (2025). Sources for individual age control points are in Table 1.

Image not available with this version

Figure 6

This image is not available with this version.

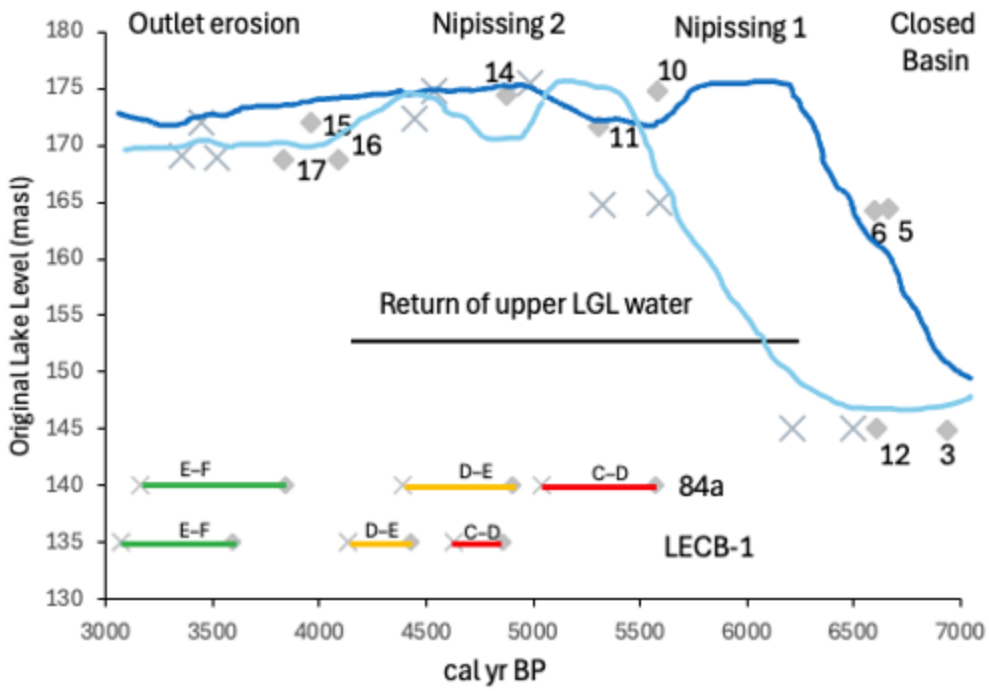


Figure 7

Relationship between IC declines and lake level**.** Lake-level curve and age constraints are modified from Lewis et al. (2012). Numbers refer to entries in SM Table 11. See the text and Figures 2 and 6 for identification of IC declines at the C–D, D–E, and E–F boundaries. The diamond symbol indicates the

maximum age of the 95.4% probability range, whereas the x symbol indicates the minimum age. Dark blue line follows lake-level interpretation of Lewis et al. (2012). Light blue line follows same interpretation but constrained by minimum of probability range. Black line showing possible time interval for return of upper LGL drainage is from Lewis et al. (2012) estimating drainage return may have begun as early as 6,300 cal yr BP and was complete by 4,190 cal yr BP.

Supplementary Files

This is a list of supplementary files associated with this preprint. Click to download.

- SaylorErieAgemodelSM.docx
- Table1.png